Effects of Thermomechanical Treatments on Pseudoelastic Strain Characteristics of Ti-29Nb-13Ta-4.6Zr for Biomedical Applications

Materials Transactions, Vol. 50, No. 7 (2009) pp. 1704 to 1712
Special Issue on New Functions and Properties of Engineering Materials Created by Designing and Processing

Effects of Thermomechanical Treatments on Pseudoelastic Strain Characteristics of Ti-29Nb-13Ta-4.6Zr for Biomedical Applications

M. Niinomi, T. Akahori, M. Nakai and H. Tsutsumi

Department of Biomaterials Science, IMR, Tohoku University, Sendai 980-8577, Japan

There is a possibility for β-type Ti-29Nb-13Ta-4.6Zr (TNTZ) to exhibit super-elastic characteristics, which is advantageous for biomedical applications such as orthodontic wires. Thermomechanical treatments are expected to induce super-elastic characteristics in β-type titanium alloys. Therefore, TNTZ specimens were subjected to various thermomechanical treatments, including solution treatments and severe cold rolling, wherein the second solution treatment temperature, second solution treatment time, and reduction ratio of cold rolling were varied in order to investigate the elastic deformation characteristics.

One of the thermomechanical treatments induces super-elastic characteristics in a TNTZ specimen. In particular, a highest total pseudoelastic strain of 2.8% is measured in the TNTZ specimen subjected to the thermomechanical treatment at a cold rolling reduction ratio of 95%, second solution treatment temperature of 1073 K, and second solution treatment time of 0.3 ks. Tensile loading and unloading stress-strain curves of the TNTZ specimens subjected to various thermomechanical treatments indicate a high total pseudoelastic strain and exhibit three step deformation process. An α'' martensite phase is formed in the TNTZ specimen subjected to the thermomechanical treatment carried out under the above mentioned conditions. [doi:10.2320/matertrans.MF200922]

(Received February 2, 2009; Accepted March 17, 2009; Published May 13, 2009)

Keywords: *β-type titanium alloy, superelastic behavior, thermomechanical treatment, biomedical applications*

1. Introduction

Titanium alloys are used in various fields because of high specific strength and excellent corrosion resistance. They exhibit shape memory effect (SME)[1] depending on their constituent elements and thermomechanical treatments that they are subjected to. TiNi,[2] Cu system alloys,[3] and iron system alloys[4] are well known as shape memory alloys (SMAs).[1] However, only TiNi has been put to practical use because it has excellent not only shape memory characteristics but also mechanical properties, corrosion resistance, workability, and wear resistance. TiNi is used in manufacturing consumer goods such as glass frames, brassieres, and antennas for cell phones. TiNi is also used in medical devices because of excellent corrosion resistance. However, it contains a large amount of Ni, which is a high risk element from the viewpoint of metal allergies. Therefore, new Ni-free shape memory alloys have been and are still being developed.

Super-elastic characteristics such as a considerably higher pseudoelastic strain than that observed in ordinary alloys can be induced in addition to the shape memory effect in shape memory alloys by heat treatments. Since super-elastic characteristics are beneficial for medical and dental fields such as for making guide wires of catheters and orthodontic wires, research and development on new functional materials showing super-elastic characteristics at a temperature between room and body temperatures for biomedical applications is desired.

Recently, a lot of Ni-free β-type shape memory titanium alloys,[5] have been developed as new metallic biomaterials, which will be able to replace TiNi. The super-elastic characteristics of these alloys are attributed to deformation-induced martensite transformation. The temperature for the occurring of super-elastic characteristics of commonly used super-elastic devices are controlled to be room temperature through thermomechanical treatments. On the other hand, Gum Metal™,[6] which exhibits only super-elastic characteristics, will be useful in biomedical devices, because its constituent elements are non-toxic and non-allergy causing. Gum Metal™ has been reported to show super-elastic characteristics under as-cold working conditions, and its deformation mechanism has been reported to be different from that of conventional shape memory alloys.

Since the chemical composition of Ti-29Nb-13Ta-4.6Zr (TNTZ),[7] which has been newly developed for biomedical applications, is similar to that of Gum Metal™, there is a possibility of TNTZ showing super-elastic characteristics. A cold wire drawing process, including a short solution treatment, was employed to make orthodontic wires of TNTZ with diameters of 1 mm and 0.3 mm. These TNTZ wires were deformed by cold swaging, and they exhibited super-elastic behavior.[7] The mechanism for this super-elastic behavior is still unclear.

Therefore, in this study, instead of cold swaging, TNTZ was subjected to severe cold rolling including solution treatment wherein the severe cold rolling and solution treatment conditions were varied. The elastic behaviors of TNTZ subjected to the various severe cold rolling and solution treatments, namely thermomechanical treatments, were then examined.

2. Experimental Procedures

2.1 Materials and thermomechanical treatments

The materials used in this study were hot forged bars of Ti-29Nb-13Ta-4.6Zr (TNTZ) with a diameter of 20 mm.

The thermomechanical treatment in this study was optimized by including the cold rolling process and short solution treatment, and it is schematically shown in Fig. 1. TNTZ subjected to the thermomechanical treatment shown in Fig. 1 is referred to as $TNTZ_B$. During this thermomechanical treatment, the second solution treatment temperature, which is the solution treatment carried out after severe cold

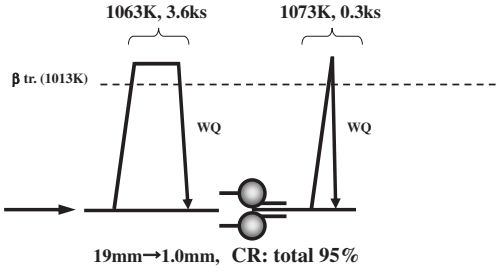

Fig. 1 Schematic drawing of basic thermomechanical treatment for TNTZ.

rolling, the second solution treatment time, and the reduction ratio of severe cold rolling were varied, as schematically shown in Figs. 2, 3, and 4. The second solution treatment temperature was varied between 673 K and 1073 K. TNTZ subjected to these thermomechanical treatments are referred to as $TNTZ_{673\,K}$, $TNTZ_{983\,K}$, $TNTZ_{1043\,K}$, and $TNTZ_{1073\,K}$ ($= TNTZ_B$), respectively. The β transus temperature of TNTZ is 1013 K. The second solution treatment time was varied between 0.01 ks and 1.8 ks. TNTZ subjected to these thermomechanical treatments are referred to as $TNTZ_{0.01\,ks}$, $TNTZ_{0.06\,ks}$, $TNTZ_{0.3\,ks}$ ($= TNTZ_B$), $TNTZ_{0.6\,ks}$, $TNTZ_{1.2\,ks}$,

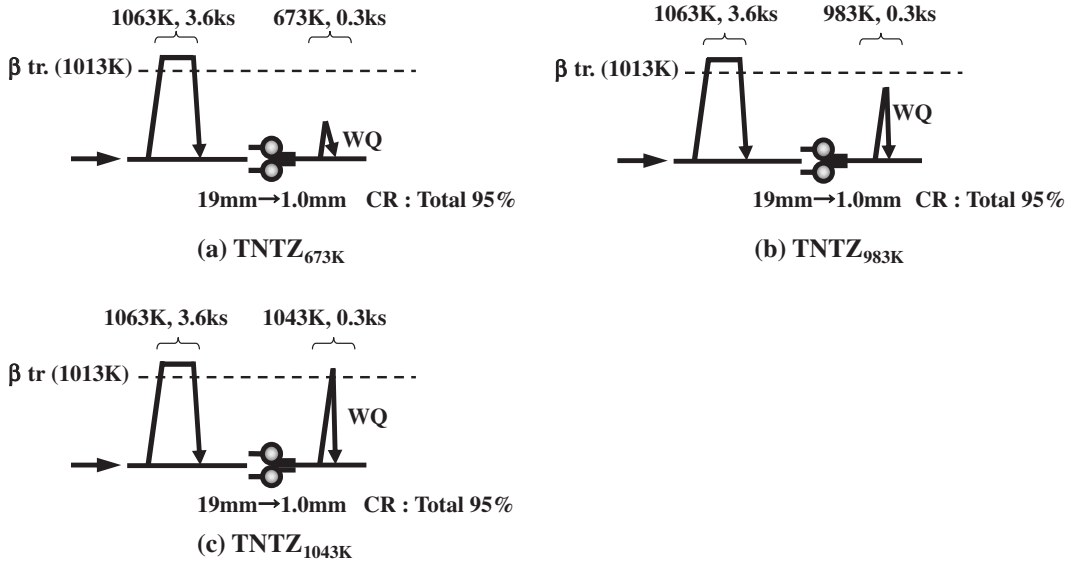

Fig. 2 Schematic drawings of thermomechanical treatments for TNTZ wherein second solution treatment temperature is changed: (a) 673 K, (b) 983 K, and (c) 1043 K.

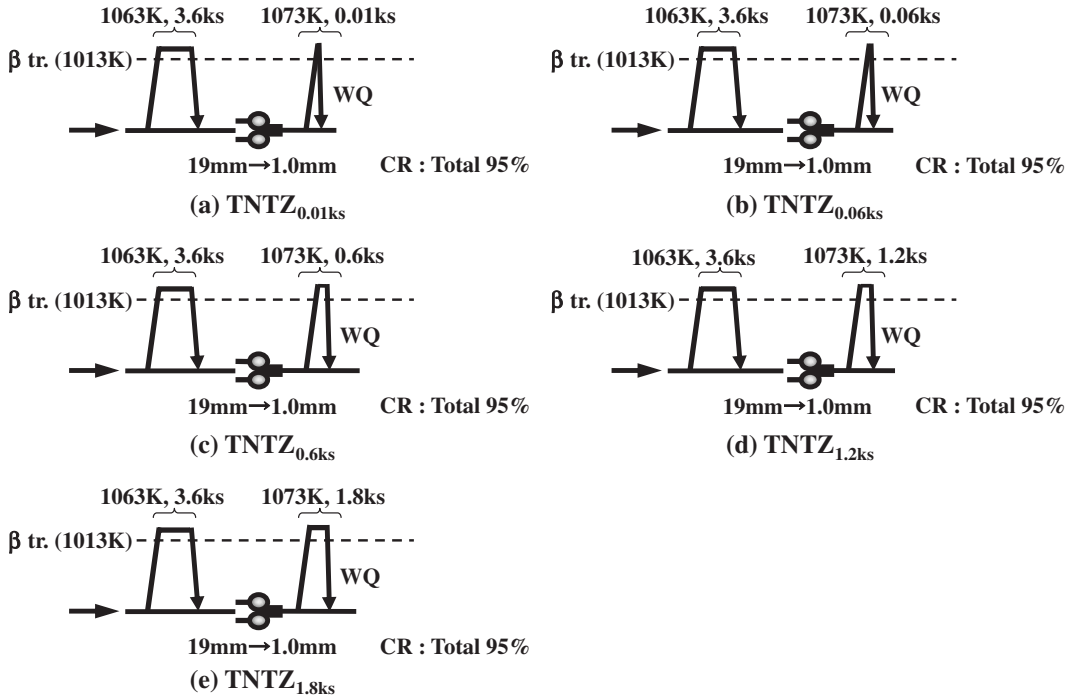

Fig. 3 Schematic drawings of thermomechanical treatments for TNTZ wherein second solution treatment time is changed: (a) 0.01 ks, (b) 0.06 ks, (c) 0.6 ks, (d) 1.2 ks, and (e) 1.8 ks.

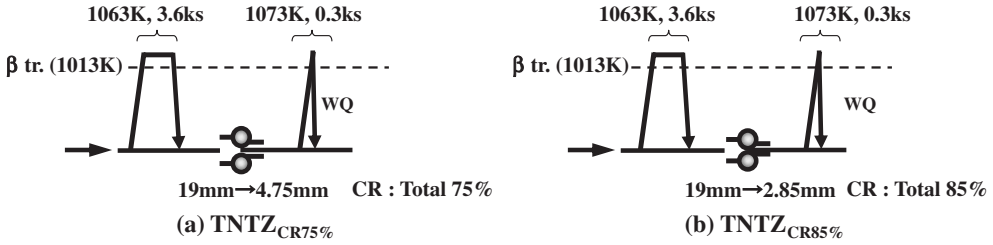

Fig. 4 Schematic drawings of thermomechanical treatment for TNTZ wherein reduction ratio of cold rolling is changed: (a) 75% and (b) 85%.

and TNTZ$_{1.8\,k}$, respectively. The reduction ratio of severe cold rolling was varied between 75% and 95%. TNTZ subjected to these thermomechanical treatments are referred to as TNTZ$_{75\%}$, TNTZ$_{85\%}$, and TNTZ$_{95\%}$ (= TNTZ$_B$), respectively. Every solution treatment was carried out in vacuum. For solution treatment in this study, the silica tube with specimen under vacuum conditions was inserted in the heated furnace at a set solution temperature and the solution time was measured when the temperature of the specimen was reached to the set solution temperature. Then the specimen was pulled out from the silica tube followed by water quenching after a set solution time.

2.2 Evaluation of super-elastic characteristics

Plates having a length of 60 mm, whose longitudinal direction was parallel to the rolling direction, were machined from TNTZ subjected to the various thermomechanical treatments. Tensile specimens with a length of 60 mm, gauge length of 10 mm, width of 3 mm, and thickness of 1.5 mm were machined from the plates along the rolling direction. The tensile specimens were subjected to tensile loading and unloading tests after wet-polishing their gauge sections using emery papers up to #1500 grids.

The tensile loading and unloading tests were carried out using an Instron type machine at a cross-head speed of 8.33×10^{-6} m/s (a strain rate of 8.33×10^{-2} s^{-1}) in ambient atmosphere. The load was measured using a load cell attached to the testing machine, while the strain was measured using both a foil strain gauge attached directly to the gauge section of the specimen and a noncontact extensometer. Under tensile loading conditions, a strain of 0.5% was continuously loaded and unloaded up to a total strain of 4.0%. Tensile loading and unloading stress-strain curves were recorded using an X-Y recorder.

2.3 Microstructural observations

The TNTZ specimens subjected to each thermomechanical treatment were cut parallel to the rolling surface in order to observe the microstructure using an optical microscope. The specimens were embedded in resin, wet-polished using emery papers up to #1500 grids, buff-polished with alumina powder and SiO_2 suspension liquid, and finally etched in 5%HF solution.

2.4 Analysis of constituent phases by X-ray diffraction

An analysis of the constituent phases of the TNTZ specimens subjected to each thermomechanical treatment before and after the pseudoelastic strain measurement test was carried out using an X-ray diffractometer (XRD) with Cu-K_α line operated at an accelerating voltage of 40 kV and a tube current of 30 mA.

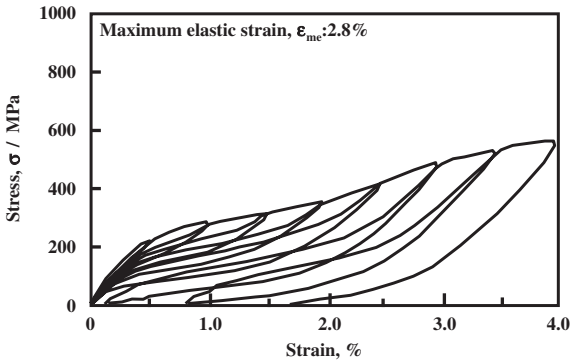

Fig. 5 Tensile loading-unloading stress-strain curves of TNTZ$_{1073\,K}$.

3. Results and Discussion

3.1 Tensile loading and unloading stress-strain curves

3.1.1 Pseudoelastic characteristics of TNTZ subjected to basic thermomechanical treatment (TNTZ$_B$)

Figure 5 shows the tensile loading and unloading stress-strain curves of TNTZ$_B$ (= TNTZ$_{1073\,K}$, TNTZ$_{0.3\,ks}$, and TNTZ$_{95\%}$). Stress increased nonlinearly with strain in the pseudoelastic strain region of the loading and unloading stress-strain curves of TNTZ$_B$. This deformation behavior was similar to that of Ti-Nb-Sn system alloys[10] showing super-elastic behavior. Residual strain was not observed in the loading and unloading stress-strain curve of TNTZ$_B$ when a strain of 2.5% was added. Thus, TNTZ$_B$ showed super-elastic characteristics. When a strain over 2.5% was added, residual strain was observed in the loading and unloading stress-strain curves. Residual strains of 0.2% and 1.7% were observed for added strains of 3.0% and 4.0%, respectively. The maximum pseudoelastic strain (ε_{me}) of TNTZ$_B$ was 2.8%.

3.1.2 Change in pseudoelastic strain characteristics with second solution treatment temperature

Figure 6 shows the tensile loading and unloading stress-strain curves of TNTZ subjected to thermomechanical treatments wherein the second solution treatment was varied: TNTZ$_{673\,K}$, TNTZ$_{983\,K}$, TNTZ$_{1043\,K}$, and TNTZ$_{1073\,K}$. The difference in the tensile loading and unloading stress-strain curves was clearly observed. In the case of TNTZ$_{673\,K}$, stress increased almost linearly with strain in the pseudoelastic strain region. In the case of TNTZ$_{983\,K}$, stress increased nonlinearly with strain in the pseudoelastic strain region.

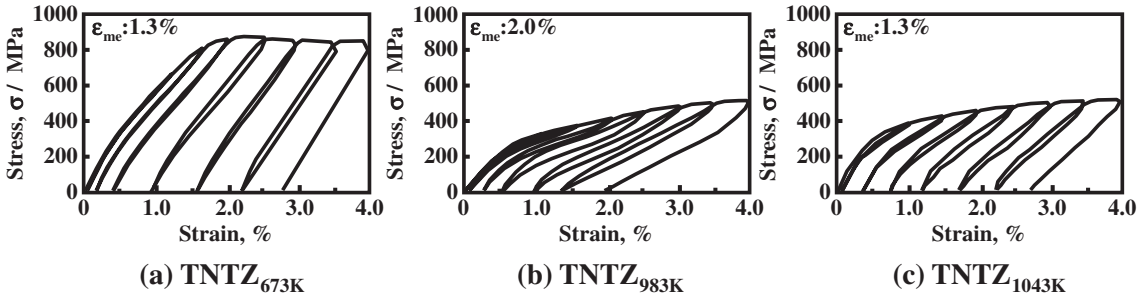

Fig. 6 Tensile loading-unloading stress-strain curves of TNTZ subjected to thermomechanical treatments for wherein second solution treatment temperature is changed: (a) 673 K, (b) 983 K, and (c) 1043 K.

However, in this case, residual strain was observed for an added strain over 2.0%. In the case of $TNTZ_{1043\,K}$, nonlinear behavior was observed in the tensile loading and unloading stress-strain curves, but residual strain was observed for an added strain below 1.0%.

Figure 7 shows the relationship between the second solution treatment temperature and ε_{me}. ε_{me} of $TNTZ_{673\,K}$, $TNTZ_{983\,K}$, and $TNTZ_{1043\,K}$ were 1.3%, 2.0%, and 1.3%. ε_{me} varied with the second solution treatment temperature. ε_{me} of $TNTZ_{673\,K}$ and $TNTZ_{1043\,K}$ was nearly equal to that of TNTZ subjected to a standard aging treatment after solution treatment. Therefore, ε_{me} of $TNTZ_{1073\,K}$ (= $TNTZ_B$) was the highest.

3.1.3 Change in pseudoelastic strain characteristics with second solution treatment time

Figure 8 shows the loading and unloading stress-strain curves of TNTZ subjected to thermomechanical treatments wherein the second solution treatment time was varied: $TNTZ_{0.01\,ks}$, $TNTZ_{0.06\,ks}$, $TNTZ_{0.3\,ks}$, $TNTZ_{0.6\,ks}$, $TNTZ_{1.2\,ks}$, and $TNTZ_{1.8\,k}$. Stress increased nonlinearly with strain in every case, but the shape of the tensile loading and unloading stress-strain curve changed with the second

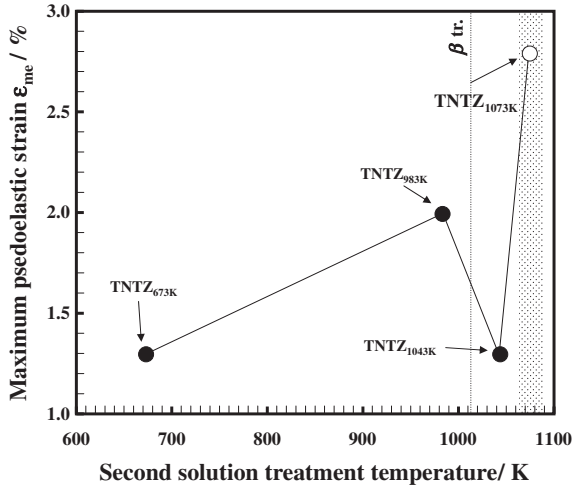

Fig. 7 Relationship between maximum psedoelastic strain, ε_{me}, and second solution treatment temperature. β tr. indicates β transus.

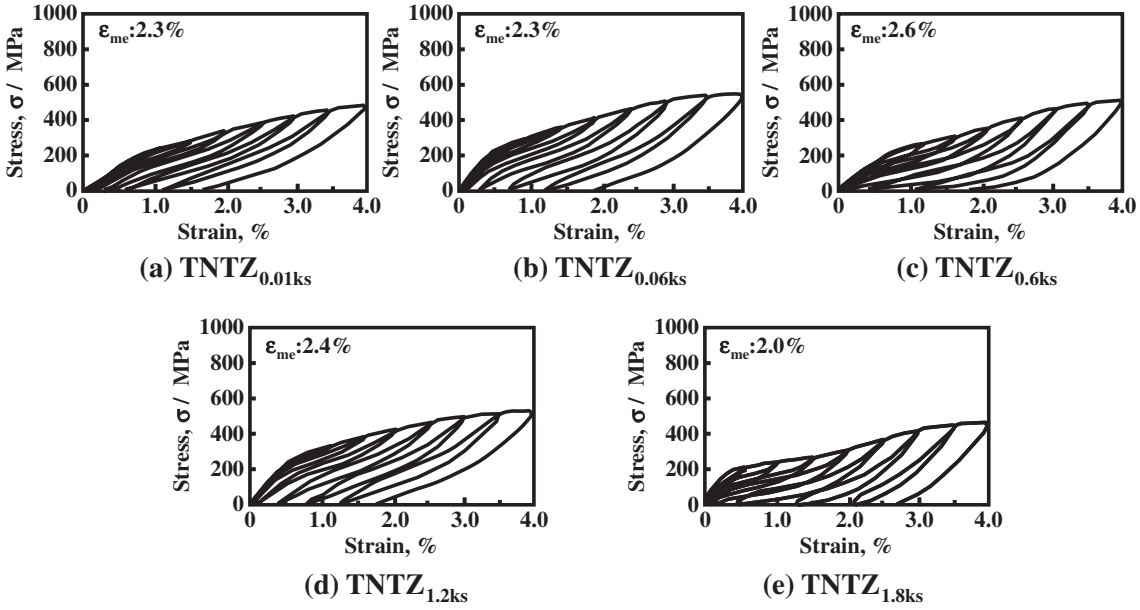

Fig. 8 Tensile loading-unloading stress-strain curves of TNTZ subjected to thermomechanical treatments wherein second solution treatment time is changed: (a) 0.01 ks, (b) 0.06 ks, (c) 0.6 ks, (d) 1.2 ks, and (e) 1.8 ks.

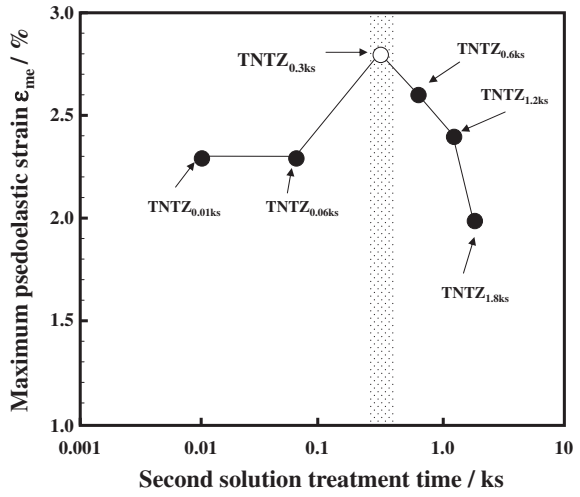

Fig. 9 Relationship between maximum psedoelastic strain, ε_{me}, and second solution treatment time.

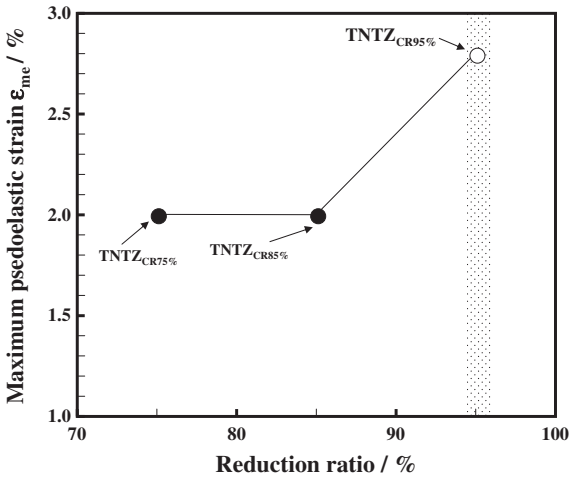

Fig. 11 Relationship between maximum psedoelastic strain, ε_{me}, and reduction ratio.

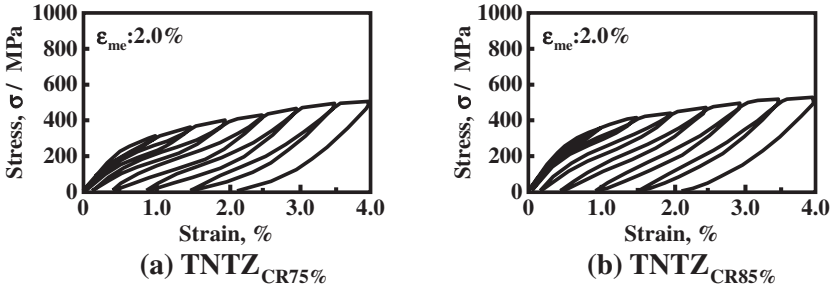

Fig. 10 Tensile loading-unloading stress-strain curves of TNTZ subjected to thermomechanical treatments wherein reduction ratio of cold rolling is changed: (a) 75% and (b) 85%.

solution treatment time. The shape of the loading and unloading stress-strain curves of $TNTZ_{0.6\,ks}$ and $TNTZ_{1.8\,ks}$ was similar to that of $TNTZ_{0.3\,ks}$, showing three step deformation process, but the tensile loading and unloading stress-strain curves of $TNTZ_{0.01\,ks}$, $TNTZ_{0.06\,ks}$, and $TNTZ_{1.2\,ks}$ did not exhibit three step deformation process. The gradient of the tensile loading and unloading stress-strain curves of $TNTZ_{1073\,K}$, $TNTZ_{0.6\,ks}$, and $TNTZ_{1.8\,ks}$ changed in the strain regions of 0%∼0.5%, 0.5%∼2.0%, and 2.0%∼4.0%, but the gradient of loading and unloading stress-strain curves of $TNTZ_{0.06\,ks}$ and $TNTZ_{1.2\,ks}$ changed in the strain ranges of 0%∼0.5% and 0.5%∼4.0%. ε_{me} of $TNTZ_{0.01\,ks}$, $TNTZ_{0.06\,ks}$, $TNTZ_{0.6\,ks}$, $TNTZ_{1.2\,ks}$, and $TNTZ_{1.8\,ks}$ were 1.5%, 2.0%, 2.5%, 1.5%, and 1.5%, respectively. Only ε_{me} of $TNTZ_{0.6\,ks}$ was nearly equal to that of $TNTZ_B$ (= $TNTZ_{0.3\,ks}$).

Figure 9 shows the relationship between the second solution treatment time and ε_{me}. ε_{me} of $TNTZ_{0.01\,ks}$ and $TNTZ_{0.06\,ks}$ was 2.3%. ε_{me} of $TNTZ_B$ (= $TNTZ_{0.3\,ks}$) was the highest.

3.1.4 Change in pseudoelastic strain characteristics with reduction ratio of cold rolling

Figure 10 shows the tensile loading and unloading stress-strain curves of TNTZ subjected to thermomechanical treatments wherein the reduction ratio of cold rolling was varied: $TNTZ_{75\%}$ and $TNTZ_{85\%}$.

The shapes of the tensile loading and unloading stress-and strain curves of $TNTZ_{75\%}$ and $TNTZ_{85\%}$ were similar to each other but were different from that of $TNTZ_B$ (= $TNTZ_{95\%}$). ε_{me} of $TNTZ_{CR75\%}$ and $TNTZ_{CR85\%}$, whose curves did not exhibit residual strain, was 1.5%.

Figure 11 shows the relationship between the reduction ratio and ε_{me}. ε_{me} of $TNTZ_{75\%}$ and $TNTZ_{85\%}$ were 2.0% and 2.0%, respectively. ε_{me} of $TNTZ_B$ (= $TNTZ_{95\%}$) was the highest. The high reduction ratio of the cold rolling ratio maybe enhances the formation of the texture leading to the high psedoelastic strain.[8)]

3.2 Microstructure

3.2.1 Change in microstructure with second solution treatment temperature

Figures 12 and 13 show optical micrographs and X-ray diffraction profiles of $TNTZ_{1073\,K}$ (= $TNTZ_{0.3\,ks}$ and $TNTZ_{95\%}$) measured before (Fig. 13(a)) and after (Fig. 13(b)) the loading and unloading tests. The microstructure of $TNTZ_{1073\,K}$ showed a matrix of the matrix recrystallized equiaxed grains whose average diameter ($\bar{d}$) was 19 μm. An orthorhombic martensite α'' phase was observed in the β phase of $TNTZ_{1073\,K}$ (= $TNTZ_{0.3\,ks}$ and $TNTZ_{95\%}$), as shown in Figs. 12(a) and (b). Peaks of β and α'' phases were observed in the X-ray diffraction profiles measured before the loading tests, as shown in Fig. 13(a).

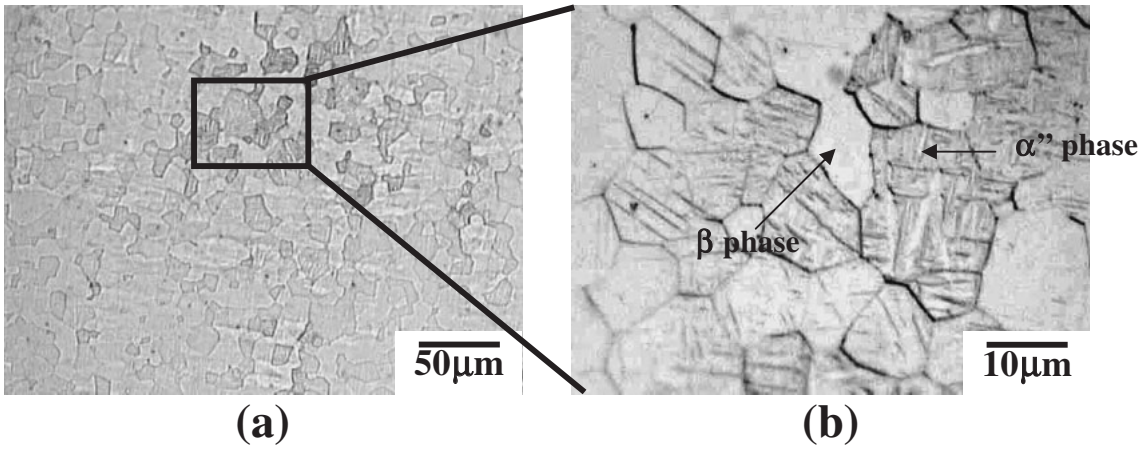

Fig. 12 Optical micrographs of TNTZ subjected to basic thermomechanical treatment: (a) Optical micrograph before tensile loading and unloading test (low magnification), and (b) Optical micrograph before tensile loading and unloading test (high magnification)

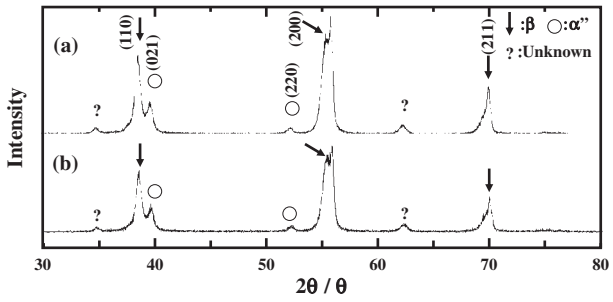

Fig. 13 X-ray diffraction profiles of TNTZ subjected to basic thermomechanical treatment: (a) Before tensile loading-unloading test (b) and After tensile loading-unloading test

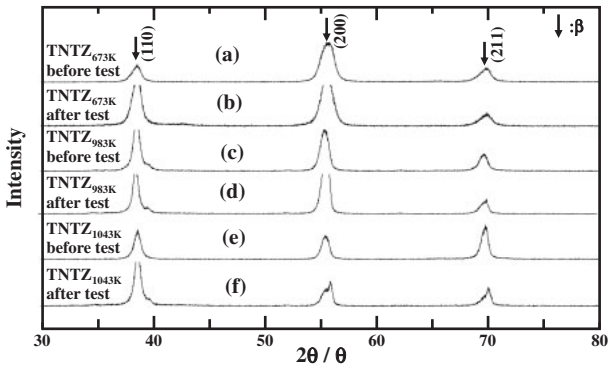

Fig. 15 X-ray diffraction profiles of TNTZ conducted with thermomechanical treatments wherein second solution treatment temperature is changed to be 673 K, 983 K, and 1043 K before (a), (c), and (e), and after (b), (d), and (f) tensile loading and unloading tests.

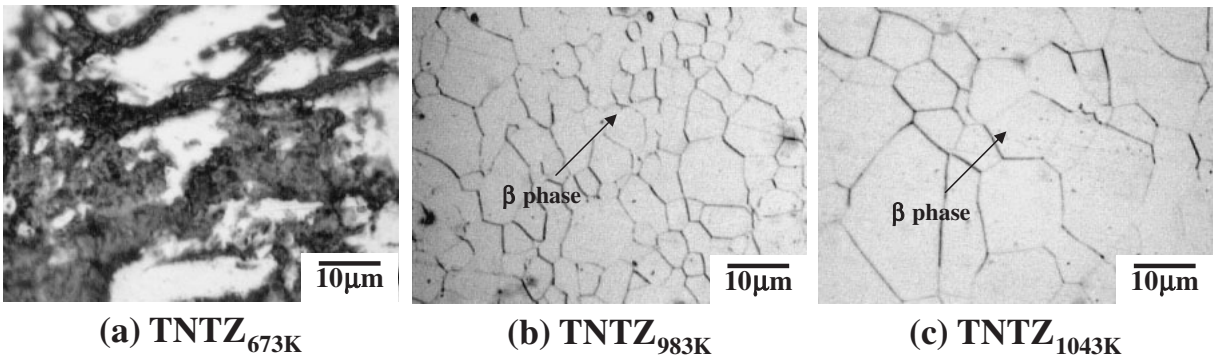

Fig. 14 Optical micrographs of TNTZ conducted with thermomechanical treatments wherein second solution treatment temperature is changed to be (a) 673 K, (b) 983 K, and (c) 1043 K, respectively before tensile tensile loading and unloading tests.

Peaks of β and α'' phases were also observed in the X-ray diffraction profiles measured after the loading test, as shown in Fig. 13(b), but their intensities were the same as those measured before the loading test.

The microstructure of TNTZ before cold rolling consisted of only a single β phase. α'' phase was not observed in the microstructure of TNTZ before cold rolling. Therefore, the formation of an α'' phase is considered to be induced by cold rolling and second solution treatment.

Figures 14 and 15 show optical micrographs and X-ray diffraction profiles of $TNTZ_{673\,K}$ $TNTZ_{983\,K}$, and $TNTZ_{1043\,K}$ measured before (Figs. 15(a), (c), and (e)) and after (Figs. 15(b), (d), and (f)) the loading and unloading tests. The deformed structure due to cold rolling was retained in the microstructure of $TNTZ_{673\,K}$. The microstructures of $TNTZ_{983\,K}$ and $TNTZ_{1043\,K}$ exhibited fine recrystallized equiaxed grains with average grain diameters ($\bar{d}$) of 14 μm and 18 μm, respectively. α'' phase was not observed in the

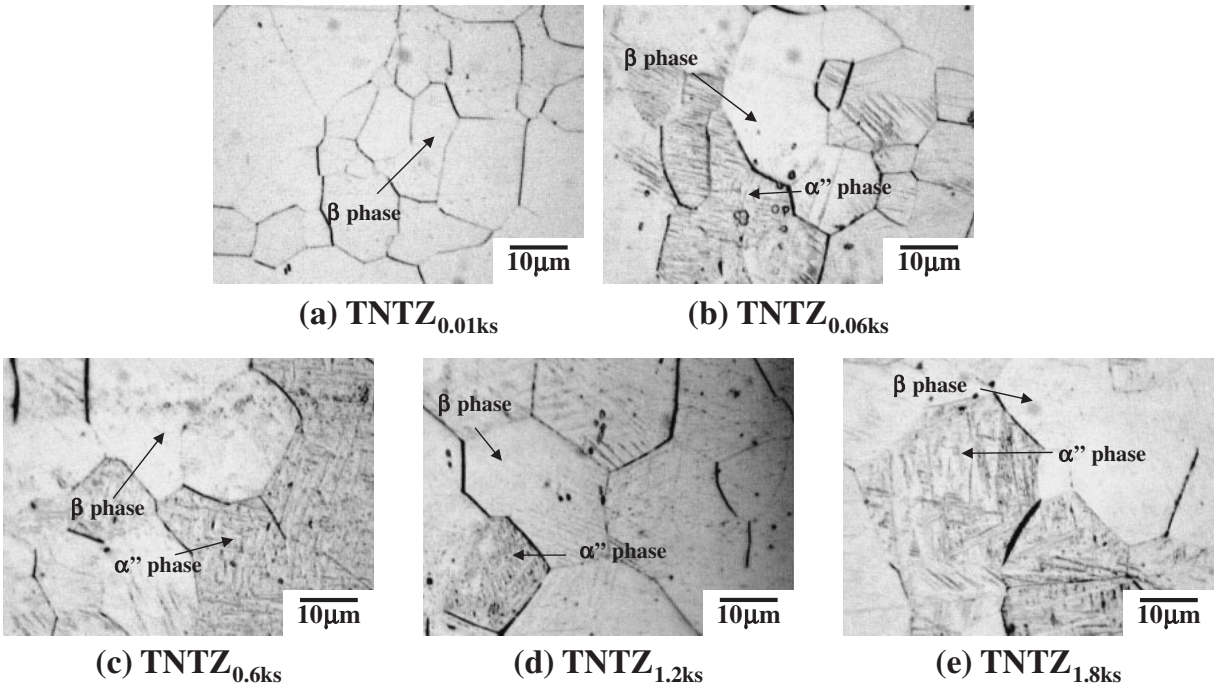

Fig. 16 Optical micrographs of TNTZ subjected to thermomechanical treatments wherein second solution treatment time is changed to be (a) 0.01 ks, (b) 0.06 ks, (c) 0.6 ks, (d) 1.2 ks, and (e) 1.8 ks, respectively before tensile loading and unloading tests.

microstructures of $TNTZ_{983\,K}$ and $TNTZ_{1043\,K}$. Muneki *et al.*[9] have reported that a large volume of α'' phase is observed in the β phase when an alloy is subjected to solution treatment at a temperature higher than its β transus temperature. Since the α'' phase was formed in $TNTZ_{1073\,K}$, its formation was considered to be enhanced by the second solution treatment carried out at a temperature over 1073 K.

Only peaks of β phase were observed in the X-ray profiles of $TNTZ_{673}$, $TNTZ_{983\,K}$, and $TNTZ_{1043\,K}$ measured before and after the loading and unloading tests.

3.2.2 Change in microstructure with second solution treatment time

Figures 16 and 17 show optical micrographs and X-ray diffraction profiles of $TNTZ_{0.01\,ks}$, $TNTZ_{0.06\,ks}$, $TNTZ_{0.6\,ks}$, $TNTZ_{1.2\,ks}$, and $TNTZ_{1.8\,ks}$ measured before (Figs. 17(a), (c), (e), (g), and (i)) and after (Figs. 17(b), (d), (f), (h), and (j)) the tensile loading and unloading tests. The microstructures of $TNTZ_{0.01\,ks}$, $TNTZ_{0.06\,ks}$, $TNTZ_{0.6\,ks}$, $TNTZ_{1.2\,ks}$, and $TNTZ_{1.8\,ks}$ exhibited fine recrystallized grains with average diameters ($\bar{d}$) of 17 μm, 19 μm, 22 μm, 25 μm, and 27 μm, respectively. α'' phases were observed in the microstructures of $TNTZ_{0.06\,ks}$, $TNTZ_{0.6\,ks}$, $TNTZ_{1.2\,ks}$, and $TNTZ_{1.8\,ks}$ but were not observed in the microstructure of $TNTZ_{0.01\,ks}$. Only peaks of β phase were observed in the X-ray diffraction profiles of $TNTZ_{0.01\,ks}$ and $TNTZ_{0.06\,ks}$ measured before and after the tensile loading and unloading tests. Thus, the volume of α'' phase in $TNTZ_{0.06\,ks}$ was very small. Peaks of α'' phase were observed in the X-ray diffraction profiles of $TNTZ_{0.6\,ks}$, $TNTZ_{1.2\,ks}$, and $TNTZ_{1.8\,ks}$ measured before and after the tensile loading and unloading tests, and their intensities remained nearly equal before and after the tensile loading and unloading tests.

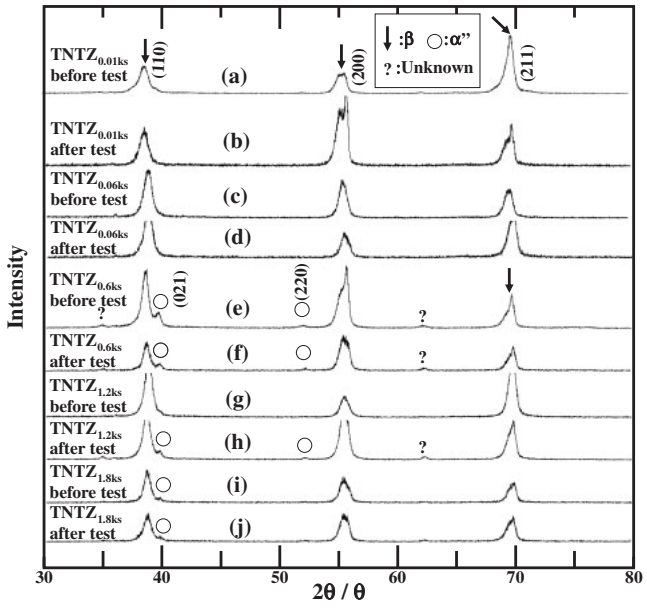

Fig. 17 X-ray diffraction profiles of TNTZ subjected to thermomechanical treatments wherein second solution treatment time is changed to be 0.01 ks, 0.06 ks, 0.6 ks, 1.2 ks, and 1.8 ks, respectively before (a), (c), (e), (g), and (i), and after (b), (d), (f), (h), and (j) tensile loading and unloading tests.

3.2.3 Change in microstructure with reduction ratio of cold rolling

Figures 18 and 19 show optical micrographs and X-ray diffraction profiles of $TNTZ_{75\%}$ and $TNTZ_{85\%}$ measured before (Figs. 19(a) and (c)) and after (Figs. 19(b) and (d)) the tensile loading and unloading tests. The microstructures of $TNTZ_{75\%}$ and $TNTZ_{85\%}$ exhibited fine recrystallized equiaxed grains with average diameters ($\bar{d}$) of 22 μm and 20 μm,

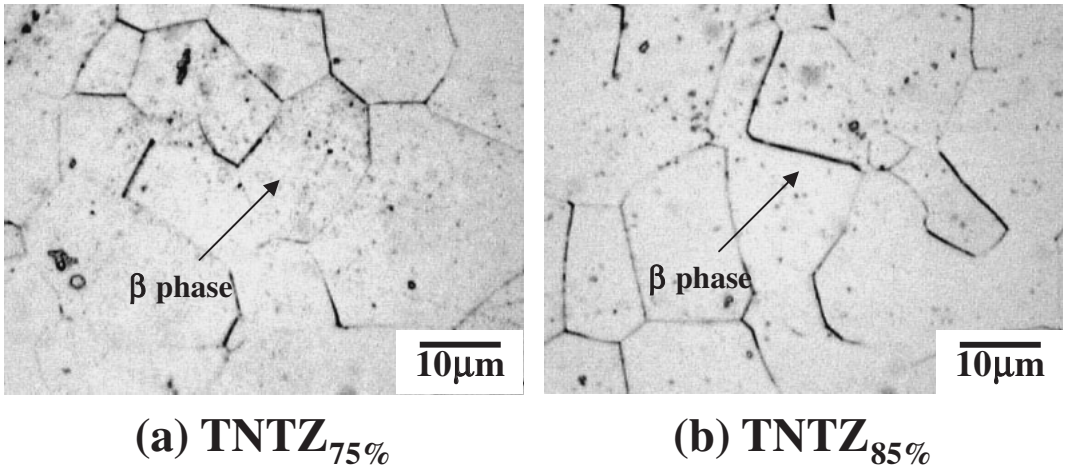

Fig. 18 Optical micrographs of TNTZ subjected to thermomechanical treatments wherein reduction ratio of cold rolling is changed to be (a) 75% and (b) 85%, respectively before tensile loading and unloading tests.

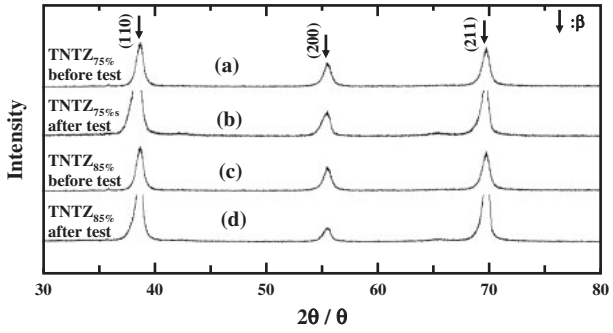

Fig. 19 X-ray diffraction profiles of TNTZ conducted with thermomechanical treatments wherein reduction ratio of cold rolling is changed to be 75% and 85%, respectively before (a) and (c), and after (b) and (f) tensile loading and unloading tests.

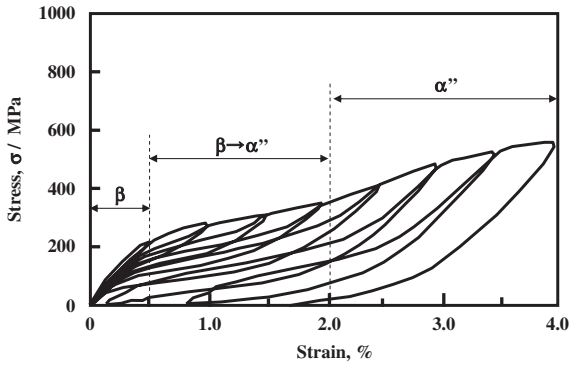

Fig. 20 Schematic drawings of tensile loading and unloading stress-strain curves of TNTZ showing high total elastic strains.

respectively. α'' phases were not observed in the profiles of $TNTZ_{CR75\%}$ and $TNTZ_{CR85\%}$.

3.3 Mechanism of pseudoelastic deformation in TNTZ showing high total pseudoelastic strain

The shapes of the tensile loading and unloading stress-strain curves of $TNTZ_B$ (= $TNTZ_{1073\,K}$, $TNTZ_{0.3\,ks}$, and $TNTZ_{95\%}$), $TNTZ_{0.6\,ks}$, and $TNTZ_{1.8\,ks}$ showing high total pseudoelastic strains were different from those of the stress-strain curves of other TNTZ showing low total pseudoelastic strains; the microstructures of $TNTZ_B$ (= $TNTZ_{1073\,K}$, $TNTZ_{0.3\,ks}$, and $TNTZ_{95\%}$), $TNTZ_{0.6\,ks}$, and $TNTZ_{1.8\,ks}$ exhibited a duplex structure of β and α'' phases. Therefore, the α'' phase seems to affect the pseudoelastic deformation behavior of the alloy. However, currently, the detailes of this effect is unclear. Further investigations are required to clarify this point.

The tensile loading and unloading stress-strain curves of $TNTZ_B$ (= $TNTZ_{1073\,K}$, $TNTZ_{0.3\,ks}$, and $TNTZ_{95\%}$), $TNTZ_{0.6\,ks}$, and $TNTZ_{1.8\,ks}$ exhibited three step deformation behaviors. Their gradient changed in the strain ranges of 0%~0.5%, 0.5%~2.0%, and 2.0%~4.0%. Grosdidier *et al.*[10] have reported that the tensile stress-strain curves of metastable β-type titanium alloy shows three step deformation process: the deformation of the β phase in the low strain region, modification of the β phase to the α'' phase in the intermediate strain region, and deformation of the fully transformed α'' phase in the high strain region. In this case, deformation-induced martensite transformation from the metastable β phase to the α'' martensite phase occurs. It has also been reported[11] that the super-elastic deformations occurring in newly developed β-type titanium alloys are a result of the deformation-induced martensite transformation. However, the super-elastic behavior of Gum Metal™ has been reported to be a result of highly distorted and localized pseudoelastic strain accumulation but not deformation-induced martensite transformation. Assuming that deformation-induced martensite transformation can occur in TNTZ subjected to thermomechanical treatments that induce super-elastic characteristics, the deformation behavior observed in the tensile loading and unloading stress-strain curves can be explained as shown in Fig. 20: the deformation of the β phase in the low strain region, deformation-induced martensite transformation of $\beta \rightarrow \alpha''$ in the intermediate strain region, and deformation of the fully transformed α'' phase. However, there was no evidence of deformation-induced martensite transformation during the deformation of TNTZ. Further investigations are required to confirm this point.

4. Conclusions

Ti-29Nb-13Ta-4.6Zr (TNTZ) was subjected to various thermomechanical treatments, including solution treatments and severe cold rolling, wherein the second solution treatment temperature, second solution treatment time, and reduction ratio of cold rolling were varied. The effects of the thermomechanical treatments on the pseudoelastic deformation characteristics of TNTZ were then investigated by conducting tensile loading and unloading tests. The following results were obtained.

(1) One of the thermomechanical treatments induces superelastic characteristics in TNTZ. In particular, a highest total pseudoelastic strain of 2.8% is measured in TNTZ subjected to a thermomechanical treatment at a cold rolling reduction ratio of 95%, second solution temperature of 1073 K, and second solution treatment time of 0.3 ks.
(2) Tensile loading and unloading stress-strain curves of TNTZ subjected to the thermomechanical treatments indicate a high total pseudoelastic strain and exhibit three step deformation processs.
(3) An α'' martensite phase is formed in TNTZ subjected to a thermomechanical treatment at a cold rolling ratio over 95%, second solution treatment temperature over 1073 K, and second solution treatment time over 0.06 ks.

Acknowledgments

The authors would like to express their thanks to Daido Steel Co., Ltd. (Nagoya, Japan), for preparing the materials. This work was supported in part by the Global COE Program "Materials Integration International Center of Education and Research, Tohoku University", the Ministry of Education, Culture, Sports, Science and Technology (MEXT) (Tokyo, Japan), the project between Tohoku University and Kyusyu University on "Highly-functional Interface Science: Innovation of Biomaterials with Highly-functional Interface to Host and Parasite", MEXT (Tokyo, Japan), The Light Metal Educational Foundation, Inc. (Osaka, Japan), the cooperative research program of Institute for Materials Research, Tohoku University (Sendai, Japan), and the cooperative research program of the Advanced Research Center of Metallic Glasses, Institute for Materials Research, Tohoku University (Sendai, Japan).

REFERENCES

1) Y. Fukui, T. Inamura, H. Hosoda, K. Wakashima and S. Miyazaki: Mater. Trans. **45** (2004) 1077–1082.
2) T. Akahori, M. Niinomi, T. Higuchi and K. Morii: J. Japan Inst. Japan **67** (2003) 595–603.
3) A. Creuziger and W. C. Crone: Mater. Sci. Eng. A **498** (2008) 404–411.
4) R. A. Shakoor and F. Ahmad Khalid: JMMB **499** (2009) 411–414.
5) J. II. Kim, H. Y. Kim, H. Hosoda and S. Miyazaki: Mater. Trans. **46** (2005) 852–857.
6) J. Hwang, S. Kuramoto, T. Furuta, K. Nishino and T. Saito: J. Mater. Eng. Performance **14** (2005) 747–754.
7) M. Niinomi, T. Akahori, S. Katsura, K. Yamauchi and M. Ogawa: Mater. Sci. Eng. C **27** (2007) 154–161.
8) T. Inamura, H. Hosoda, K. Wakashima and S. Miyazaki: Mater. Trans. **46** (2005) 1597–1603.
9) S. Muneki, Y. Kawabe and J. Takahashi: J. Japan Inst. Metals **51** (1987) 916–922.
10) T. Grosdidier and M. J. Philippe: Mater. Sci. Eng. A **291** (2000) 218–223.
11) E. Takahashi, T. Sakurai, S. Watanabe, N. Masahashi and S. Hanada: Mater. Trans. **43** (2003) 2978–2983.